Flexible Alternating-Current Electroluminescence Plunging to Below 1 Hz Frequency by Triboelectrification

Yanshuo Sun, Laipan Zhu, Jin Yang, Jianjun Zhang, Baodong Chen,* and Zhong Lin Wang*

Low frequency, portable power source is one of the key challenges for applications of wearable alternating-current electroluminescent (ACEL) device because it typically requires a working frequency above 500 Hz. Here, an extremely low frequency self-powered ACEL system is proposed, which consists of a vertical contact-separation triboelectric nanogenerator and a self-made flexible ACEL device. It achieves directly-driven electroluminescence phenomenon in real-time by triboelectrification and works completely self-powered through converting kinetic energy of human body into electricity. The working frequency has fallen from 500 to 1 Hz, i.e., the real frequency needed for electroluminescence has dropped 500 times, which is due to the favorable low-frequency high-voltage advantages of the triboelectric nanogenerator. It delivers a stabilized open-circuit voltage of 160 V and a short-circuit current of 6 μA for applied force of 0.1 N. Meanwhile, a strong blueshift is also observed experimentally with the change of working frequency. Furthermore, a self-powered medical protective gown is demonstrated that is real-time monitoring both the temperature and humidity. This work breaking the bottleneck of high-frequency driving, demonstrates the great potential of self-powered ACEL systems in wearable electronics and medical health.

1. Introduction

Electroluminescence (EL), a kind of non-thermal light produced by electric field, has been developed and applied as an important part in flexible lighting displays, human-machine interactions, and intelligent electronic skin.[1–10] Typically, EL is a luminescence phenomenon that converts electrical energy into light, including injection EL and intrinsic EL, which are classified into two categories: high-field EL and low-field EL.

The basic structure of high-field EL is an alternating-current electroluminescent (ACEL) device, where the electrons in the phosphor or injected by the electrode are accelerated in the crystal and collide with the luminescent center to excite or ionize under the applied electric field, and emit radio light when electrons return to the ground state.[11,12] Compared to the traditional LED, the ACEL device has attracted widespread concerns due to its low power consumption, long service life, and excellent mechanical stability, however, the high frequency and unavoidable high driving voltage required for light-emitting limits the wide application in smart wearable field. Meanwhile, with the rapid development of science and technology, electronic devices have shown a trend of miniaturization, low power consumption, and multi-function, thus it is urgent to find a low carbon, environmentally friendly, and clean energy to get rid of the dependence on traditional power sources.

Pioneered by Wang and co-workers, nanogenerators based on the coupling of the triboelectrification and electrostatic induction have been developed in the last few years,[13–15] ushering a new era of environmental energy collection and utilization. Unlike traditional chemical batteries, which have a limited lifespan and need to be replaced or recharged frequently.[16–18] The TENG have shown unprecedented output performance and advantages in harvest randomly distributed or irregular mechanical energy from the environment into electrical energy,

Y. Sun, L. Zhu, J. Yang, J. Zhang, B. Chen, Z. L. Wang
Beijing Institute of Nanoenergy and Nanosystems
Chinese Academy of Sciences
Beijing 101400, P. R. China
E-mail: chenbaodong@binn.cas.cn

Y. Sun, J. Yang, J. Zhang
College of Chemistry and Chemical Engineering
Center on Nanoenergy Research
School of Physical Science and Technology
Guangxi University
Nanning 530004, P. R. China

The ORCID identification number(s) for the author(s) of this article can be found under https://doi.org/10.1002/adom.202101918.

L. Zhu, B. Chen, Z. L. Wang
School of Nanoscience and Technology
University of Chinese Academy of Sciences
Beijing 100049, P. R. China

B. Chen
Institute of Applied Nanotechnology
Jiaxing, Zhejiang 314031, P. R. China

Z. L. Wang
CUSTech Institute
Wenzhou, Zhejiang 325024, P. R. China

Z. L. Wang
School of Materials Science and Engineering
Georgia Institute of Technology
Atlanta, GA 30332-0245, USA
E-mail: zlwang@gatech.edu

ADVANCED
SCIENCE NEWS
www.advancedsciencenews.com

ADVANCED
OPTICAL
MATERIALS
www.advopticalmat.de

such as ocean waves,[19,20] winds,[21,22] and human-body movements.[23,24] In contrast to driving direct-current electronic devices or electrochemical reactions, TENG can drive ACEL devices easily without rectification circuits due to their AC compatibility. Hence, the integration of TENG and ACEL devices has been shown an effective way to improving the portability and wearability of wearable electronics, which not only effectively harvest the mechanical energy in the environment, but eliminate the energy loss during rectification, providing a more powerful platform for portable electronic devices.

Herein, we have developed an extremely low frequency, portable power source by using triboelectrification for integrating flexible self-powered ACEL system, which consists of a vertical contact-separation triboelectric nanogenerator (VCS-TENG) and an ACEL device. The breakthrough of this work is that it can be achieved to directly drive EL device by triboelectrification produced using the gently patting at the frequency of nearly 1 Hz. Another even more important is that the system is completely self-powered operating without any external power sources at all. Because of VCS-TENG based on the two opposite friction materials of Nylon and polyvinyl chloride (PVC) is fabricated, which can freely convert kinetic energy of human body into electricity. Owing to the favorable low-frequency AC characterisics of VCS-TENG and the flexibility of the device, that is easily attached to clothing, increasing practicality and security.

Its results have been aided by the intrinsic output advantages of VCS-TENG in high-voltage and lower current under larger load resistance, which delivers an open-circuit voltage of 160 V and a short circuit of 6 μA with an effective contact area of 25 cm². More to the point, while the realized minimum working frequency is just 1 Hz when the system is working properly. The working frequency has fallen from 500 to 1 Hz when the system is working properly, which AC frequency needed for EL phenomenon has dropped 500 times. Meanwhile, a strong blueshift phenomenon is also observed experimentally with the change of working frequency and open-circuit voltage. Furthermore, a self-powered medical protective gown is demonstrated successfully that is both temperature and humidity monitoring in real-time, indicating that it is used mainly in fast warning and displays the efficacy and safety of epidemic prevention and provide protection to medical staff.

2. Results and Discussions

2.1. Structure of the ACEL

In general, the basic structure of the flexible ACEL device with four layers integration is shown in **Figure 1**a and the cross-sectional SEM image of Figure 1b. It mainly consists of top
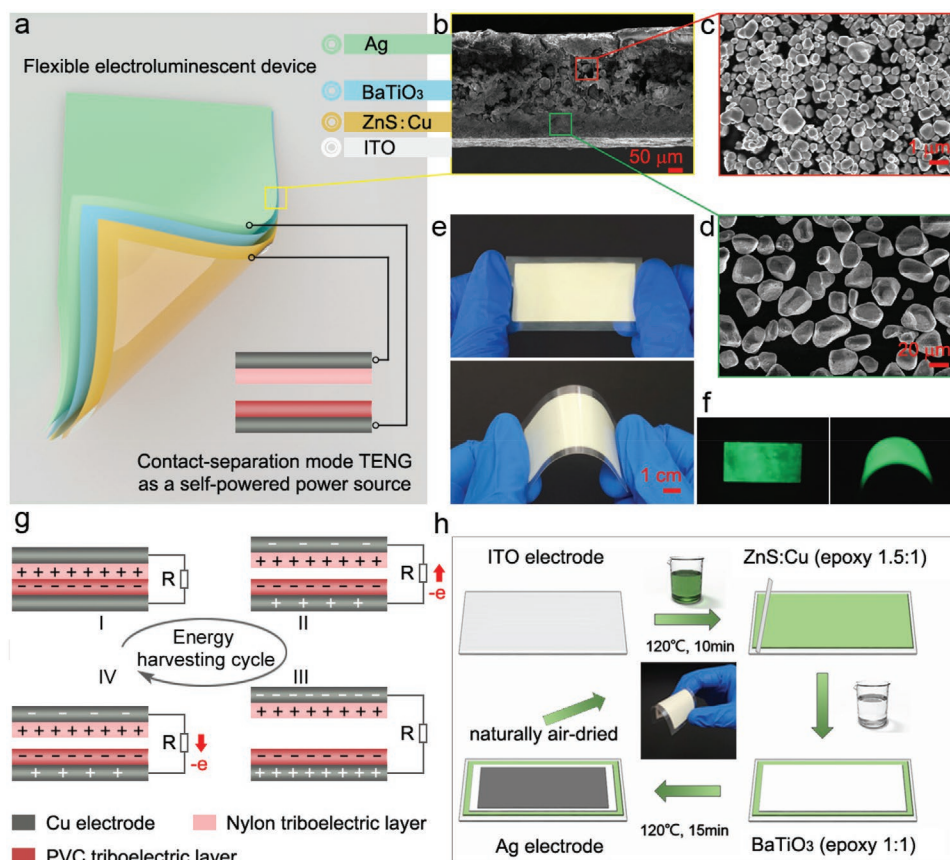

Figure 1. Structure design of the ACEL device. a) Schematic diagram showing the detailed structure of the ACEL device. b) Cross-section of the whole device. c) SEM image of BaTiO₃. d) SEM image of ZnS: Cu. e,f) Optical images of the ACEL device at original and bending. g) Schematics of the operating principle for the VCS-TENG. h) Fabrication process of the ACEL device.

**ADVANCED
SCIENCE NEWS**
www.advancedsciencenews.com

**ADVANCED
OPTICAL
MATERIALS**
www.advopticalmat.de

electrode, phosphor layer, dielectric layer, and bottom electrode respectively. For electrodes, indium tin oxide (ITO) is the most commonly used as the top electrode, which provides a series of remarkable properties including high transparency (≥80%), low resistance (6Ω sq^{-1}), flexibility, and conductivity. Silver paste or any material with excellent conductivity is an important part of the bottom electrode, which achieves arbitrary writing and electroluminescence. The middle layer is composed of phosphor layer and dielectric layer. In the phosphor layer, copper-doped zinc sulfide (ZnS: Cu) was selected as the electroluminescent luminescent material due to its outstanding chemical stability and electroluminescent properties. The morphology of the ZnS: Cu particles is shown in Figure 1d. Among them, ZnS is the main material and Cu is the center of the luminescent emitting green or blue light during excitation. Doping and co-doping with different transition metals is a key way to prepare inorganic luminescent materials, which can be easily adjusted by doping with different concentrations and types of elements. For instance, Manganese (Mn), Chromium (Cr), and Erbium (Er) can also be used as doping metals as luminescent centers are excited by highly accelerated electrons, resulting in emitting light corresponding to respective energy bands. The dielectric layer is composed of barium titanate (BaTiO$_3$) and epoxy resin. BaTiO$_3$ is the most popular insulating material due to its extremely high dielectric constant (2000–3000 at room temperature). It has been reported that nanoscale BaTiO$_3$ enhance the brightness of electroluminescent device,[25–27] so we used ultrasonic method to reduce the size to avoid agglomeration. The SEM image is shown in Figure 1c. As a binder, epoxy resin not only promotes to form a dense and uniform layer of BaTiO$_3$, but also enhances the dielectric coefficient of the dielectric layer. The existence of the dielectric layer mainly plays a protective role to prevent the short circuit of the electroluminescent device caused by the fluorescence quenching due to the high field intensity.

In addition, the ACEL device exhibits excellent EL performance, which emits light under the bending state (Figure 1e,f). Figure 1h indicates the ACEL device was fabricated by an easy and simple method of blade-coating method (see Experimental Section for details), resulting in the thin thickness (391 μm) and light-weight (0.892 g) under the area of 4 cm × 2.5 cm (Figures S1 and S2, Supporting Information). Due to the thinness and lightness, ACEL devices are more conducive to wearable integration and portability. Besides, Figure 1g illustrates the working principles of the VCS-TENG, which is in conjunction with triboelectrification and electrostatic induction. Owing to the simple structural design, an alternating current will be generated through the continuous contact and separation movements between the Nylon and PVC polymeric materials.

2.2. Electrical Output Performance of VCS-TENG

A photograph of a contact-separation structured VCS-TENG unit is shown in **Figure 2**a, which consists of Cu as the metal electrodes, a layer of Nylon as an electrification material with a thickness of 25 μm, PVC as another dielectric layer, where its thinness would enhance the wearability and contribute to the portability of the device. Through COMSOL, the potential

distributions in the contact and separation states are simulated accordingly to observe the power generation processes (Figure 2b). Figure 2c and Movie S1, Supporting Information, demonstrate that the VCS-TENG could light up 80 LEDs in series through tapping. In order to evaluate the effective electrical output performance of the VCS-TENG, a linear motor was used to provide periodic contact-separation motion to investigate the output performance of the VCS-TENG at different frequencies. As demonstrated in Figures 2d,f, the VCS-TENG can effectively capture the energy in a frequency range of 0.5–2.5 Hz, which generate a high output performance (V_{oc}: 160 V, I_{sc}: 6 μA) under a contact area of 25 cm2 and applied force of 0.1 N (Figure S3, Supporting Information), and the current increases with frequency, voltage and charge output does not change significantly. This is explained by the fact that a faster contact-separation motion means that there will be more contact release cycles per unit time, resulting in a larger current. Figure 2g shows that in the force range of 1–5 N, the open-circuit voltage gradually increases as the contact force increases. In addition, we measured the output current at different resistances. The maximum output current of VCS-TENG gradually decreases as the external resistance increases. At the same time, the corresponding instantaneous power is 0.418 mW maximum at a load resistance of 300 MΩ (Figure 2h). In addition, in order to evaluate the stability of VCS-TENG, we tested the output performance of the VCS-TENG after 5000 vertical contact-separation cycles at a frequency of 1 Hz, the output voltage changes minimally (Figures 2i), indicating the high durability of the VCS-TENG for long term operations.

As a wearable device, comfortable and compatibility are very important for long-term usage. Therefore, we have tested the bending performance of ACEL device and demonstrated superior stability and excellent EL performance. During the experiment, the ACEL device was fixed at one end of the linear motor to test the stability in repeated motion conditions. As shown in **Figure 3**a,b, the emission intensity just led to a small decrease of 7.6% in the emission intensity even after 1000 bending cycles tests at a frequency of 1 Hz, which indicates that the ACEL device possess well bending stability and excellent luminous performance. Meanwhile, the ACEL device with different patterns can be fabricated by blade-coating method (Figure 3c). In the ACEL device, the light-emitting wavelength and luminous intensity are rigidly related to the frequency and the driving voltage. Therefore, the emitting light colors and luminous intensity can be easily tuned by changing the frequency and magnitude of the applied voltage. However, due to the works for a long time at a condition of high voltage and high frequency, the performance of the ACEL device will be affected that the brightness increase and shorten the life.[6] Therefore, the relationship between the luminous brightness and various applied voltages of ACEL device can be expressed by

$$L = L_0 \exp(-\beta / V^{1/2}) \tag{1}$$

where L_0 and β are empirical parameters determined by the device material and structure, L is luminance, V is the applied voltage. The normalized EL spectra of the ACEL device under different frequencies (0.5–2.5 Hz) are exhibited in Figure 3d,f. Figure 3e shows the associated optical image where
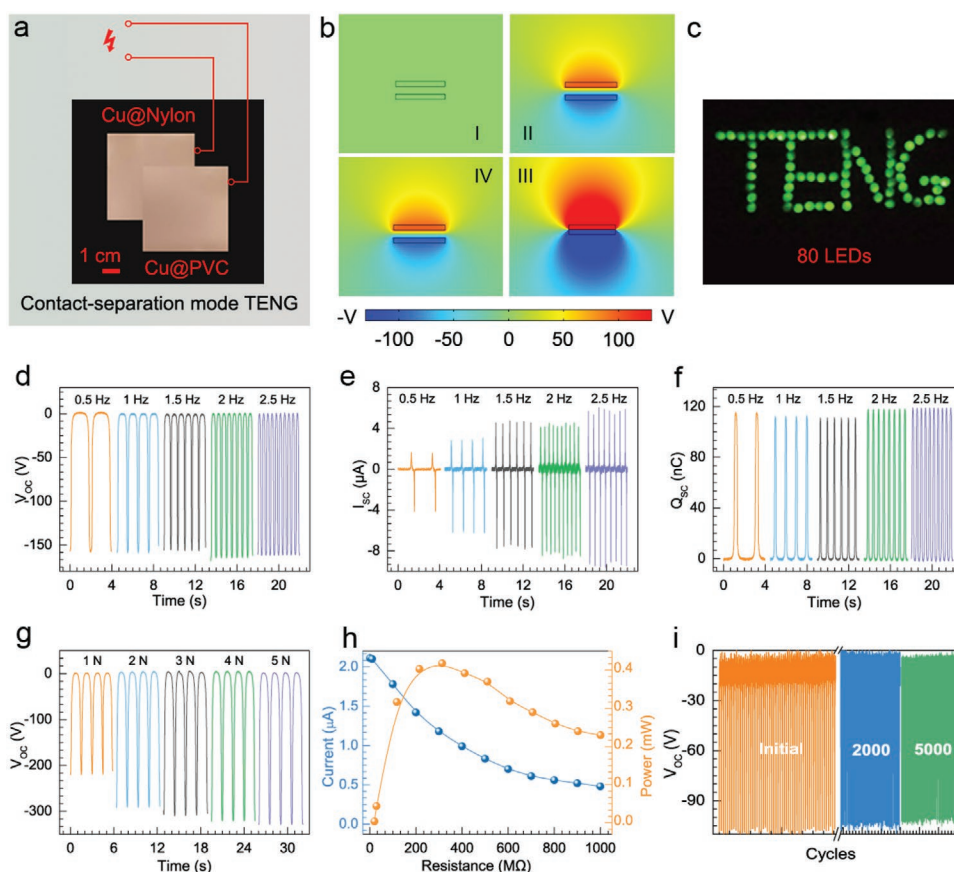
**ADVANCED
SCIENCE NEWS**

www.advancedsciencenews.com

**ADVANCED
OPTICAL
MATERIALS**

www.advopticalmat.de

Figure 2. Output performance of the TENG in vertical contact-separation mode. a) Optical images of VCS-TENG. b) Potential simulation by COMSOL to elucidate the working principle. c) The photograph of 80 LEDs lighted by hand tapping of the VCS-TENG. d–f) Open-circuit voltage, short-circuit current, and short-circuit transferred charges at various frequencies of the VCS-TENG (0.5–2.5 Hz). g) Open circuit voltages of VCS-TENG under different forces (1–5 N). h) The output current and power of the VCS-TENG under various load resistance. i) Output electrical stability of VCS-TENG under long-time cycling.

the brightness of the ACEL device increases as the frequency increases. Upon increasing the frequency from 0.5 to 2.5 Hz, the EL emission peak showed a blue shift with the emission peak maximum shifted from 521 to 518 nm (Figure 3f). Meanwhile, the relationship between the brightness of the ACEL device and the applied voltage is shown in Figure 3g,h. It can be seen that the luminous intensity increases with driving voltage increasing, which is attributed to the augment in the energy and number of excited hot electrons due to the improvement in the driving voltage, which increases the electron transit from excited state to ground state, resulting in the increases of luminous intensity. The result also demonstrates the relationship between luminous intensity and driving voltage. Figure 3i depicts that ACEL device exhibits an emission peak at 519 nm under a certain frequency and the luminous intensity increases rapidly with the increasing applied voltage.

2.3. The Electroluminescent Mechanism via TENG

As illustrated in **Figure 4**a, the ACEL device is composed of a phosphors layer that is sandwiched between the conductive layer and dielectric layer. At present, the theory inorganic EL is

yet to be further studied as its not fully mature, while the ACEL device mainly relies on the excitation of electric fields including impact ionization or impact excitation theory.[28,29] The collision excitation is due to the direct collision between hot electrons and the luminescent center as schematically illustrated in Figure 4b. First, the deep-level electrons in the phosphor layer interface or dielectric layer are excited to enter the phosphor layer by tunneling under the driving high field. The initial electrons are accelerated to become hot electrons, caused the electron energy transition from the ground state to the excited state via the collision with the EL center. As the electrons return from the excited state to the ground state, the energy is released in the form of light, and uncaptured hot electrons are trapped as space charges on the interface between the anode side of the insulating layer and light-emitting layer. It can be seen that EL is a complex physical process including interface emission, electron transport, collision excitation, and field ionization, which are interlinked and affect each other. The emitted light is transmitted from a highly transparent electrode substrate and the devices are expected to be used in large-area light sources and instrumentation display panels.

The results in Figure 4c,d shows the CIE color coordinates of the ACEL device at different driving voltages, from which it can
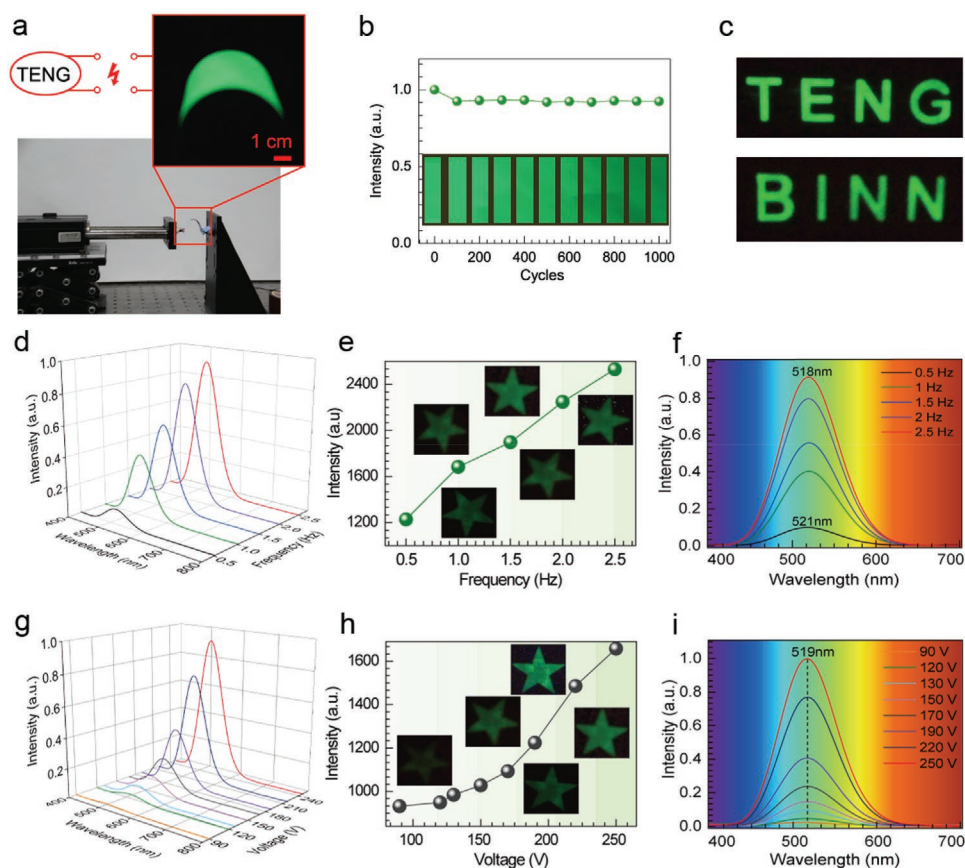
Figure 3. Optical properties of ACEL device. a,b) The brightness intensity of the ACEL device with the bending cycles. c) Patterned ACEL device. d–f) EL spectra of ZnS: Cu at various applied frequencies (0.5–2.5 Hz). g–i) EL spectra and the relative intensity of ACEL device under various voltage, the corresponding photographs are shown in the inset.

be seen more intuitively that the coordinates gradually move from the light green area to the dark green area as the driving voltage increases, which also verifies the experimental results that the intensity of luminescence increases as the increase in voltage. Meanwhile, the chromaticity coordinates shift gradually from green towards blue in color space as the frequency increases from 0.5 to 2.5 Hz, which can be clearly observed in the 1931 chromaticity diagram (Figure 4f,g). The shift in peak position is attributed to the difference in application frequency, since the emission intensity and color are strongly dependent on the application frequency. As the frequency increases, the corresponding EL centers excited by the electric field and the EL intensity increases consequently. The main reason for the blue shift is due to the particularity of the ZnS: Cu energy level structure, which exists two different acceptor levels of Cu leads to a change in EL color. One is the deep acceptor level far from the valence band, corresponding to the green EL center as shown in Figure 4e. The other is the shallow acceptor level closer to the valence band of ZnS, where the holes at the energy level are easily relaxed into the valence band to produce fluorescence quenching, corresponding to the blue EL center as shown in Figure 4h. At the low-frequency excitation, the holes in the blue EL center relax to the valence band or the green EL center during the half-period excitation due to the hole's life is shorter than the half excitation period. Thus, the holes in the

green EL center become the main ionization center and play a major role in the EL. Under the excitation of high frequency, the hole in the blue EL center become the dissociation center during excitation half-period, which increases the specific gravity compared to the holes in the green EL center without relaxation, so the blue component of the emission increased, resulting in the emission peak blue shift.

2.4. Applications in Medical Health Self-Powered Monitoring

With the epidemic of the Corona Virus Disease 2019, the safety of medical personnel is of utmost importance, while the protective suit is an important barrier to reduce the risk of infection to maximize the safety of medical personnel. However, the protective suit is easily damaged after prolonged activity, medical personals are exposed to bacteria, which increases the chance of infection. So, we designed a system in which the ACEL device is integrated with VCS-TENG and simultaneously monitors temperature and humidity (**Figure 5**a). As displayed in Figure 5b, the VCS-TENG and ACEL device attached to the protective suit that the medical personnel writes on the ACEL device arbitrarily to achieve EL in real-time by patting the VCS-TENG at low frequency (nearly 1 Hz). The charging capability of the VCS-TENG with different capacitors (Figure 5d), illustrating that the
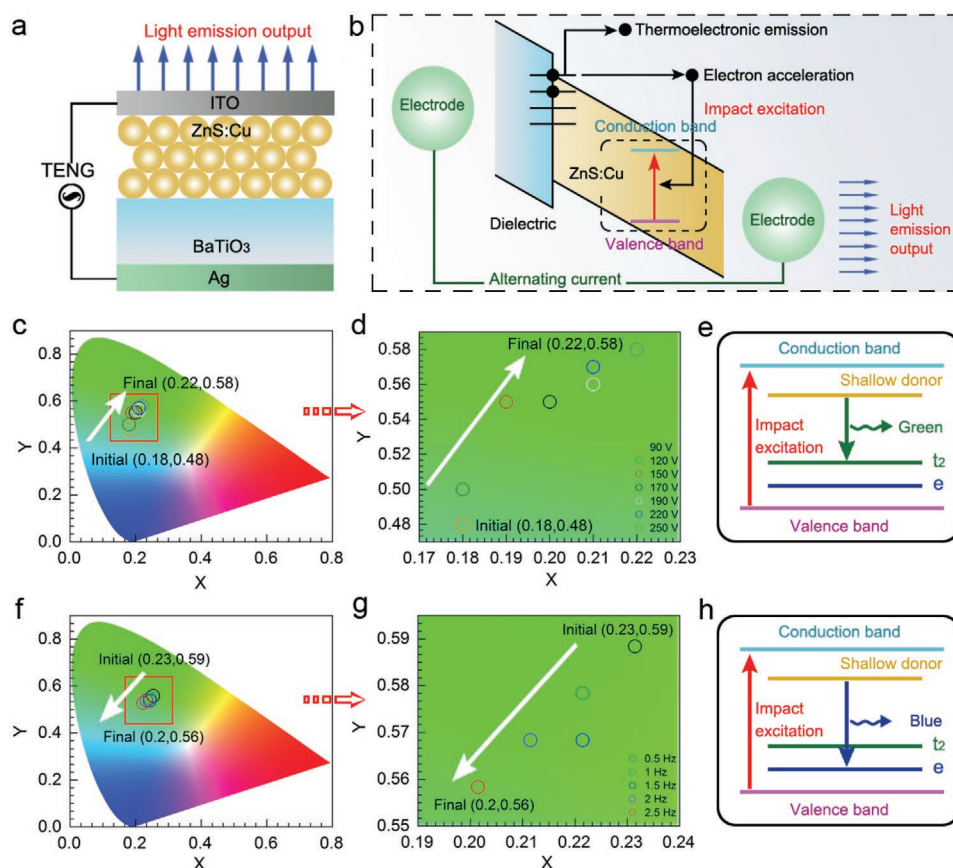
Figure 4. Structure, mechanism, and electroluminescence characteristics of ACEL device. a) Structure of ACEL device. b) The mechanism of luminescence. c,d) CIE coordinates of ACEL devices at different voltages. f,g) CIE coordinates of ACEL device at various frequencies (0.5–2.5 Hz). e,h) Schematic energy level diagram of electronic transitions.

charging rate gradually accelerated as the capacitance decreases. Besides, the collected power can be rectified and stored in a capacitor or battery for later use through rectification. Figure 5c and Movie S2, Supporting Information, demonstrate the VCS-TENG which generates high voltage, low current, and AC compatibility that can directly drive ACEL device to emit green light, which can be observed clearly in the dark. Meanwhile, temperature and humidity sensors are placed in the protective suit, which monitors the temperature and humidity changes in real-time by the monitoring system (Figure 5e and Figure S5, Supporting Information). The monitoring system works normally when the protective suit is in normal condition, while as the protective suit is damaged (Figure 5f), the temperature and humidity indications drop dramatically leading to the triggering of an alarm, as shown in Figure 5e, Figure 5f and Movie S3, Supporting Information. Advanced technologies have a significant impact on modern healthcare monitoring systems, such as the internet of things (IOT) and cloud computing, which provide statistics and analysis from massive data to contribute to remote healthcare monitoring, alerting, and making important medical indications. Thus, the system illustrates the feasibility of medical health self-powered monitoring, based on the significant advantages of ACEL device in terms of flexibility, thinness, stability, and integration, which has a promising prospect in wearable integrated device systems.

3. Conclusion

In summary, an extremely low frequency, wearable, self-powered ACEL system has been achieved based on triboelectrification, which consists of a VCS-TENG and an ACEL device. This technologies breakthrough significance is that it can be achieved to directly drive EL phenomenon in real-time by triboelectrification produced using the gently patting at the frequency of nearly 1 Hz, which is due to the favorable low-frequency high-voltage AC output advantages of VCS-TENG. Another even more important point is that the system is completely self-powered operating without any external power sources at all, because VCS-TENG can freely convert kinetic energy of human body into electricity. These results confirmed that the working frequency has fallen from 500 Hz to 1 Hz when the system is working properly, which AC frequency needed for EL phenomenon has dropped 500 times. Meanwhile, a strong blueshift phenomenon is also observed experimentally with the change of working frequency and open-circuit voltage. Furthermore, owing to the intrinsic flexibility advantages of VCS-TENG and EL device, that is easily attached to clothing, increasing practicality and security. A self-powered medical protective gown is demonstrated successfully that is real-time both temperature and humidity monitoring, indicating that it is used mainly in fast warning and display the efficacy and safety
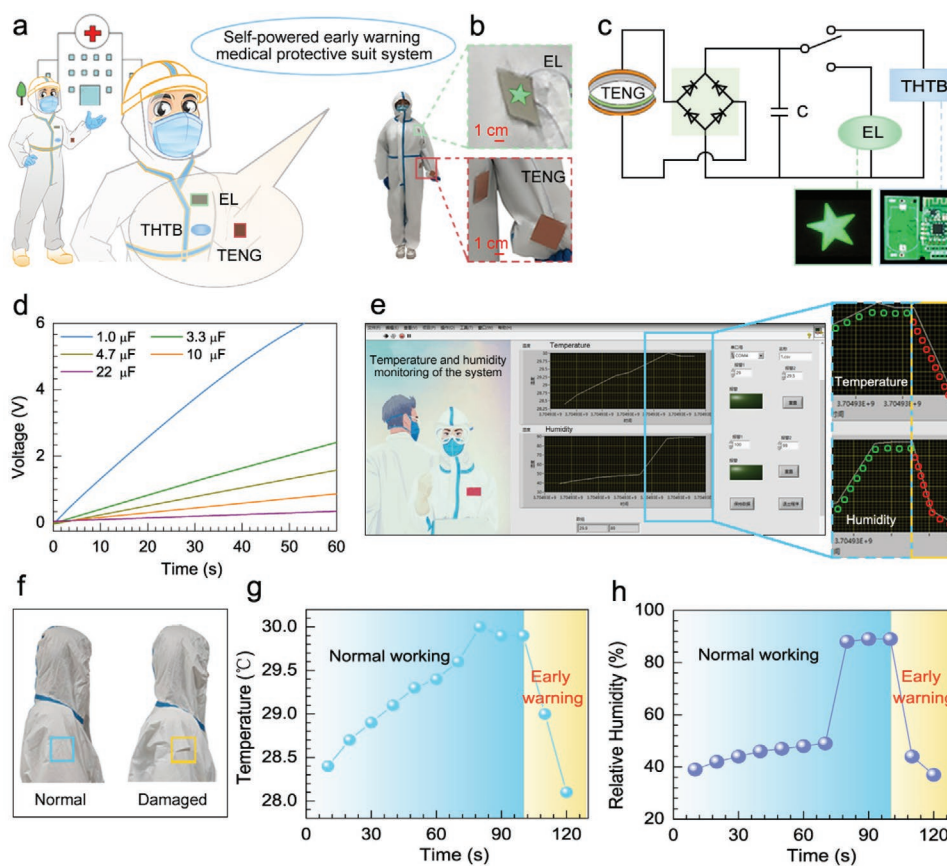
Figure 5. Demonstration of the developed VCS-TENG with ACEL device in medical health self-powered monitoring. a) Corresponding application scenario diagram. b) Picture showing the ACEL device integrated with TENG are attached on the protective suit. c) Schematic diagram of various self-powered intelligent electronic devices driven by VCS-TENG. d) Charging curve of the TENG at various capacitance capacities. e) Screenshot showing the temperature and humidity sensing system. f) Partial schematic diagram of protective suit. g,h) Monitored changes in temperature and humidity data.

of epidemic prevention and provide protection to medical staff. This work breaking the bottleneck of high-frequency driving, demonstrating the great potential of self-powered ACEL system based on TENGs in wearable electronics and medical health monitoring.

4. Experimental Section

Fabrication of ACEL Device: The flexible ACEL device was fabricated by a simple blade-coating method consisting of two electrodes, a phosphor layer and a dielectric layer. First, the phosphor layer was prepared by mixing phosphor (ZnS: Cu) with epoxy resin in the ratio of 1.5:1, and then it was repeatedly scraped twice on the ITO electrode and dried in an oven at 120 °C for 10 min. Next, $BaTiO_3$ and epoxy resin were mixed in a ratio of 1:1 and scraped on the phosphor layer after 30 min of ultrasonic method, and then dried in an oven at 120 °C for 15 min three times. Finally, a layer of silver paste or any conductive materials was scraped on the dielectric layer, thus contract the ACEL device.

Fabrication of VCS-TENG: A vertical contact-separation mode TENG was fabricated based on two different films of Nylon and PVC friction layers. A layer of Nylon as an electrification material with a thickness of 25 μm, PVC as another electrification material with a thickness of 100 μm, the copper as the electrode with a size of 5 cm × 5 cm, which adhered on 3 M foam tape to serves as a buffer cushion.

Characterization and Measurement: The morphologies of luminescent powder (ZnS: Cu), dielectric powder ($BaTiO_3$), and the cross-sectional images of ACEL device were measured by field emission scanning electron microscopy (Nova Nano 450). The EL spectrum was tested through a compact spectrometer. A linear motor was used to provide periodic contact-separation motion to produces output voltage and short-circuit current, which were measured by a programmable electrometer (Keithley, model 6514). The monitoring system was constructed based on LabView, which was capable of realizing real-time temperature and humidity data acquisition.

Supporting Information

Supporting Information is available from the Wiley Online Library or from the author.

Conflict of Interest

The authors declare no conflict of interest.

Data Availability Statement

Research data are not shared.

Keywords

[1] F. Stauffer, K. Tybrandt, *Adv. Mater.* **2016**, *28*, 7200.

[2] Y. Zhou, S. Cao, J. Wang, H. Zhu, J. Wang, S. Yang, X. Wang, D. Kong, *ACS Appl. Mater. Interfaces* **2018**, *10*, 44760.

[3] W. Lee, H. K. Lyu, H. S. Cho, S. E. Lee, B. Choi, *J. Lumin.* **2020**, *220*, 117015.

[4] M. Kneissl, T. Y. Seong, J. Han, H. Amano, *Nat. Photonics* **2019**, *13*, 233.

[5] A. Yakoh, W. Siangproh, O. Chailapakul, N. Ngamrojanavanich, *ACS Appl. Mater. Interfaces* **2020**, *12*, 22543.

[6] H. Fang, H. Tian, J. Li, Q. Li, J. Dai, T. L. Ren, G. Dong, Q. Yan, *Nano Energy* **2016**, *20*, 48.

[7] J. Wang, C. Yan, K. J. Chee, P. S. Lee, *Adv. Mater.* **2015**, *27*, 2876.

[8] H. Shin, B. K. Sharma, S. W. Lee, J. B. Lee, M. Choi, L. Hu, C. Park, J. H. Choi, T. W. Kim, J. H. Ahn, *ACS Appl. Mater. Interfaces* **2019**, *11*, 14222.

[9] D. H. Lien, M. Amani, S. B. Desai, G. H. Ahn, K. Han, J. H. He, J. W. Ager3rd, M. C. Wu, A. Javey, *Nat. Commun.* **2018**, *9*, 1229.

[10] X. Y. Wei, X. Wang, S. Y. Kuang, L. Su, H. Y. Li, Y. Wang, C. Pan, Z. L. Wang, G. Zhu, *Adv. Mater.* **2016**, *28*, 6656.

[11] B. Lee, J. Y. Oh, H. Cho, C. W. Joo, H. Yoon, S. Jeong, E. Oh, J. Byun, H. Kim, S. Lee, J. Seo, C. W. Park, S. Choi, N. M. Park, S. Y. Kang, C. S. Hwang, S. D. Ahn, J. I. Lee, Y. Hong, *Nat. Commun.* **2020**, *11*, 663.

[12] K. Kuhnke, C. Grosse, P. Merino, K. Kern, *Chem. Rev.* **2017**, *117*, 5174.

[13] F. R. Fan, Z. Q. Tian, Z. L. Wang, *Nano Energy* **2012**, *1*, 328.

[14] S. Niu, S. Wang, Y. Liu, Y. S. Zhou, L. Lin, Y. Hu, K. C. Pradel, Z. L. Wang, *Energy Environ. Sci.* **2014**, *7*, 2339.

[15] X. Pu, M. Liu, L. Li, C. Zhang, Y. Pang, C. Jiang, L. Shao, W. Hu, Z. L. Wang, *Adv. Sci.* **2015**, *3*, 1500255.

[16] Y. Zou, X. Hu, H. Ma, S. E. Li, *J. Power Sources* **2015**, *273*, 793.

[17] X. Zeng, M. Li, D. Abd El-Hady, W. Alshitari, A. S. Al-Bogami, J. Lu, K. Amine, *Adv. Energy Mater.* **2019**, *9*, 1900161.

[18] Y. Zhang, F. Wan, S. Huang, S. Wang, Z. Niu, J. Chen, *Nat. Commun.* **2020**, *11*, 2199.

[19] H. Guo, Z. Wen, Y. Zi, M. H. Yeh, J. Wang, L. Zhu, C. Hu, Z. L. Wang, *Adv. Energy Mater.* **2016**, *6*, 1501593.

[20] J. R. Morber, X. Wang, J. Liu, R. L. Snyder, Z. L. Wang, *Adv. Mater.* **2009**, *21*, 2072.

[21] S.-J. Park, S. Lee, M.-L. Seol, S. B. Jeon, H. Bae, D. Kim, G.-H. Cho, Y.-K. Choi, *Nano Energy* **2019**, *55*, 115.

[22] B. Chen, Y. Yang, Z. L. Wang, *Adv. Energy Mater.* **2018**, *8*, 1702649.

[23] J. H. Park, C. Wu, S. Sung, T. W. Kim, *Nano Energy* **2019**, *57*, 872.

[24] X. Pu, M. Liu, X. Chen, J. Sun, C. Du, Y. Zhang, J. Zhai, W. Hu, Z. L. Wang, *Sci. Adv.* **2017**, *3*, e1700015.

[25] Y. Zhou, C. Zhao, J. Wang, Y. Li, C. Li, H. Zhu, S. Feng, S. Cao, D. Kong, *ACS Mater. Lett.* **2019**, *1*, 511.

[26] J. Yan, Y. Han, S. Xia, X. Wang, Y. Zhang, J. Yu, B. Ding, *Adv. Funct. Mater.* **2019**, *29*, 1907919.

[27] P. Sharma, R. G. McQuaid, L. J. McGilly, J. M. Gregg, A. Gruverman, *Adv. Mater.* **2013**, *25*, 1323.

[28] W. W. Piper, F. E. Williams, *Phys. Rev.* **1955**, *98*, 1809.

[29] W. A. D. M. Jayathilaka, A. Chinnappan, J. N. Tey, J. Wei, S. Ramakrishna, *J. Mater. Chem. C* **2019**, *7*, 5553.